# Physics-Guided Learning of Meteorological Dynamics for Weather Downscaling and Forecasting

Yingtao Luo*
Carnegie Mellon University
Pittsburgh, USA
yingtaol@andrew.cmu.edu

Shikai Fang*
Microsoft Research Asia
Beijing, China
fangshikai@microsoft.com

Binqing Wu*
Zhejiang University
Hangzhou, China
binqingwu@cs.zju.edu.cn

Qingsong Wen[†]
Squirrel Ai Learning
Bellevue, USA
qingsongedu@gmail.com

Liang Sun[‡]
DAMO Academy, Alibaba Group
Bellevue, USA
liang.sun@alibaba-inc.com

## Abstract

Weather forecasting is essential but remains computationally intensive and physically incomplete in traditional numerical weather prediction (NWP) methods. Deep learning (DL) models offer efficiency and accuracy but often ignore physical laws, limiting interpretability and generalization. We propose *PhyDL-NWP*, a physics-guided deep learning framework that integrates physical equations with latent force parameterization into data-driven models. It predicts weather variables from arbitrary spatiotemporal coordinates, computes physical terms via automatic differentiation, and uses a physics-informed loss to align predictions with governing dynamics. *PhyDL-NWP* enables resolution-free downscaling by modeling weather as a continuous function and fine-tunes pre-trained models with minimal overhead, achieving up to 170× faster inference with only 55K parameters. Experiments show that *PhyDL-NWP* improves both forecasting performance and physical consistency.

## CCS Concepts

• **Applied computing → Physical sciences and engineering**; • **Computing methodologies → Machine learning**.

## Keywords

Physics; Learning; Weather; Prediction; Parameterization

*Work done during summer internship at Alibaba Group.
[†]Work done at Alibaba Group, and now affiliated with Squirrel Ai Learning, USA.
[‡]To whom correspondence should be addressed.

## 1 Introduction

Weather prediction remains one of modern science's most complex and vital challenges, with the nonlinear interactions between various meteorological variables, the vast spatial and temporal scales involved, and the chaotic nature of weather systems. The first-principle approach to weather prediction, i.e., numerical weather prediction (NWP), relies on mathematical models of atmospheric and oceanic phenomena. NWP is often computationally intensive at high resolution, and many unresolved physical processes such as precipitation and radiation need to be represented by parameterization. Therefore, there has been a growing interest in using machine learning (ML) models for weather prediction. Deep learning models, trained by nearly 40 years of European Center for Medium-Range Weather Forecasts (ECMWF) reanalysis v5 (ERA5) data [8], have demonstrated remarkable ability to capture complex nonlinear relationships for tasks such as weather forecasting [28, 39] and downscaling [35]. However, despite the recent success of ML techniques, the application of deep learning to weather prediction is not without challenges. Existing ML models do not incorporate established physical laws (e.g., fluid dynamics, thermodynamics) to ensure that the derived variables are consistent with these laws.

Physics-Informed Neural Networks (PINN) [30] have gained prominence as alternatives to traditional numerical simulations, offering innovative approaches to weather prediction. However, weather prediction is inherently complex, involving numerous factors and processes that are influenced by local variations, boundary condition changes, small-scale phenomena like microclimates, and external forces. Many of these critical factors, which significantly affect first-principle equations, are often missing from existing datasets due to challenges in measurement and quantification. For instance, the PDE governing temperature evolution (see Table 6) includes thermal diffusivity, which is not available in typical weather datasets such as ERA5 and must instead be estimated through turbulence parameterizations. Other unavailable terms include vertical velocity, friction, etc. This poses a challenge to constructing complete and accurate physical models, thereby limiting the fidelity of physics-informed learning approaches in real-world settings.

In light of this challenge, we propose a novel framework, *PhyDL-NWP*. This proposed paradigm first trains a neural network to predict weather conditions based on spatio-temporal coordinates,

then leverages automatic differentiation for calculating partial differential equation (PDE) terms. Based on this, we construct a library of physics terms derived from first-principle equations that can be represented using available dataset variables. To address unresolved processes and missing variables, we adopt a parametrization strategy, introducing a latent force model as a parametrization term to capture the effects of physical forces not explicitly represented in the constructed PDEs.

This design enables *PhyDL-NWP* to generate super-resolution weather data at arbitrary granularity, while simultaneously providing interpretable physical insights. Based on the constructed governing equations that represent the physical principles, we constrain and guide the optimization of deep learning models, enhancing model performance across datasets with varying climates and sources. In extensive experiments across 17 baselines and four datasets, we demonstrate that the learned parameterized PDEs align closely with the desired physical equations. The physics-guided models consistently outperform their vanilla counterparts.

In short, our contributions are summarized as follows:

- We propose a novel physics-guided learning framework *PhyDL-NWP* that completes weather equations using latent force parameterization to inform deep learning models of the underlying physical mechanism of meteorology.
- *PhyDL-NWP* directly provides a novel way to model weather data in an online learning manner with unlimited granularity. Weather downscaling can be done by simply feeding any continuous coordinates to the model, without the need for coarse-granular data as input during inference.
- *PhyDL-NWP* provides an effective paradigm for weather forecasting by forcing the prediction to align with the parameterized weather equations via a physics-guided loss.
- *PhyDL-NWP* is extremely efficient and can be directly used to fine-tune any pre-trained weather forecasting model. It can be up to 170 times faster in inference than a standalone model, with only up to 55 thousand parameters.
- The state-of-the-art performance of *PhyDL-NWP* is evaluated using both reanalysis and real-world observational datasets, spanning global and local scales. *PhyDL-NWP* shows consistency with the underlying physics in a variety of weather variables.

## 2 Related Work

In the area of weather prediction, Numerical Weather Prediction (NWP) [1, 21] is the current mainstream method. It uses mathematical models of the atmosphere and oceans, such as partial differential equations (PDE), to predict future weather based on current weather conditions. Some notable NWP models include European Centre for Medium-Range Weather Forecasts (ECMWF)[1], Global Forecast System (GFS)[2], etc. NWP can forecast weather in the medium range but usually involves extensive computation. For example, ECMWF operates one of the largest supercomputer complexes in Europe.

Recently, deep learning has emerged as another promising solution to weather forecasting [9, 29] and downscaling [26, 35] tasks.

These deep learning models [7, 37] rely on different neural architectures such as LSTM [15], CNN [38], GNN [19] and Transformer [39] to capture the evolving dynamics and correlation across space and time. Many large models have emerged in recent years. For example, ClimaX [24], GraphCastNet [14], ClimateLearn [25], FengWu [3], Pangu-Weather [2] all use backbones such as the Vision Transformer (ViT), UNet and autoencoders, for training a large model for weather forecasting. WeatherBench [31] benchmarks the use of pre-training techniques for weather forecasting. In addition, FourcastNet [28] leverages the adaptive Fourier neural operator (AFNO) [5, 16] to treat weather as a latent PDE system. In recent years, a few studies such as NeuralGCM [13] and WeatherGFT [41] have started to explore the integration of underlying physical mechanisms [36] in weather prediction. However, there are still no explicit efforts to use parameterization to ensure the completeness of the primitive equations based on the data.

In addition, spatio-temporal modeling based on deep learning [18] has thrived in recent years. Many previous works also approach the weather prediction task from the perspective of spatio-temporal modeling [6]. Dynamical systems modeling involves the formulation of systems whose states evolve over time. Given the governing equations, physics-informed approaches [12, 30] use the physics mechanism to enhance the dynamical systems. In the absence of governing equations, the identification of physical equations [4, 22, 23] is proposed to provide insights with respect to the laws of physics.

## 3 Methodology

### 3.1 Problem Definition

We study a spatiotemporal weather dataset, denoted as

$$\mathbf{u} = [u_1(x, y, t), \ldots, u_h(x, y, t)]. \tag{1}$$

Using the physics expression, this dataset comprises $h$ distinct weather variable fields (such as temperature and pressure), each related to specific input coordinates $(x, y, t)$. Here, $x \in [1, \ldots, n]$ and $y \in [1, \ldots, m]$ represent spatial coordinates, while $t \in [1, \ldots, T]$ corresponds to the temporal dimension.

This dataset can be alternatively expressed as a sequence of spatial "images" $\mathbb{X} = [X_1, \ldots, X_T]$, with each "image" $X_i$ being a tensor in $\mathbb{R}^{n \times m \times h}$, encapsulating the spatial and weather-factor dimensions at each time point.

We focus on two primary tasks based on this dataset:

- **Weather Downscaling**: The goal is to generate super-resolution weather "images" $\mathbb{Y} = [Y_1, \ldots, Y_T]$ from $\mathbb{X}$, where each $Y_i$ is a tensor in $\mathbb{R}^{n' \times m' \times h}$. The challenge is to derive this detailed data from the original, coarser dataset $\mathbb{X}$, with the dimensions $n' > n$ and $m' > m$.
- **Weather Forecasting**: This task aims to find a model $g$ to predict future weather conditions for a duration of $r$ hours, represented as $[\mathbb{X}]_{i+1}^{i+r} = [X_{i+1}, \ldots, X_{i+r}]$. These predictions are based on observed data from the preceding $s + 1$ hours, $[\mathbb{X}]_{i-s}^{i} = [X_{i-s}, \ldots, X_i]$, for each time instance $i$. That is, $g([\mathbb{X}]_{i-s}^{i}) = [\mathbb{X}]_{i+1}^{i+r}$.
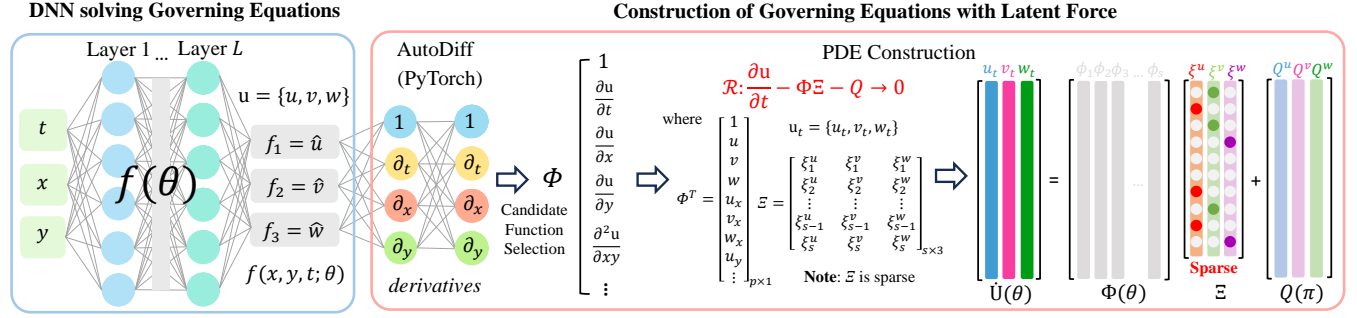
**DNN solving Governing Equations**          **Construction of Governing Equations with Latent Force**



**Figure 1: Schematic diagram of *PhyDL-NWP* for downscaling. First, given a continuous input coordinate $(x, y, t)$, the surrogate model $f_\theta$ approximates the weather data. Then, based on PyTorch's auto-differentiation and the existing meteorology theory, we calculate the derivatives for the construction of physical mechanisms driven by PDE. Last, based on linear regression, we learn the PDE that fits the weather data well to provide physical guidance.**

## 3.2 Meteorology Dynamics Representation

In this section, we aim to learn the physical mechanism represented by PDE with parameterization to fit the weather data. A typical partial differential equation (PDE) with parametrization terms has the following form:

$$\frac{\partial u}{\partial t} = Q_\pi(x, y, t) + \Phi(u)\Xi = Q_\pi(x, y, t) + \sum_{i=1}^{p} \phi(u)_i \xi_i, \quad (2)$$

where $p$ denotes the number of PDE terms in the equation, each $\phi(u)_i \in [1, u, \frac{\partial u}{\partial x}, \frac{\partial u}{\partial y}, \frac{\partial^2 u}{\partial x^2}, ..., u\frac{\partial u}{\partial x}, ...]$ denotes a PDE term in the equation (see examples in Sec. 4.3), with the set of $\xi_i$ as the coefficients. $Q_\pi(x, y, t)$ denotes the latent force modeled by a neural network that cannot be represented by $\Phi(u)$ explicitly, as a supplement to missing variables unavailable in the weather dataset, such as friction. Examples of Eq. 2 can be seen in Table 6, where a physical equation is composed of both explicit PDE terms and latent force parameterization.

## 3.3 Continuous Weather Downscaling

We develop a surrogate weather variable model $\hat{u} = f_\theta(x, y, t)$, which takes the spatio-temporal coordinates as input and predicts the $h$ weather variables. The schematic diagram of the proposed surrogate model is shown in Fig. 1. Both $f_\theta$ and $Q_\pi(x, y, t)$ are designed as feedforward neural networks that are commonly used in the PINN literature [12, 30]. The joint optimization of $f_\theta(x, y, t)$, $\phi(\hat{u})_i$, and $Q_\pi(x, y, t)$ allows the model to simultaneously learn to predict weather variables and approximate the underlying physical dynamics. Once $f_\theta$ achieves sufficient accuracy, its gradients via automatic differentiation enable the accurate calculation of PDE terms. These inferred terms, together with $Q_\pi$, in turn guide the training of $f_\theta$, ensuring physical consistency in the learned mapping.

This framework supports continuous weather downscaling in an online learning manner: once trained, $f_\theta$ can be queried with any new coordinate $(x, y, t)$ for real-time prediction. Unlike traditional downscaling methods that rely on discrete pairs of low- and high-resolution training data, *PhyDL-NWP* treats weather data as a continuous function over space-time. This enables arbitrary-resolution inference without requiring coarse-resolution inputs or pre-defined grid structures. Downscaling is performed simply by

evaluating $Y = f_\theta(x', y', t)$ at any desired fine-grained coordinates in real time, as described in Fig. 1, where $x' \in \mathbb{R}^{n'}, y' \in \mathbb{R}^{m'}$ can be any interpolation within the observed spatial domain, enabling super-resolution modeling with minimal inference cost.

The overall loss function $\mathcal{L}_D$ for weather downscaling is:

$$\mathcal{L}_D(\theta, \Xi, \pi) = \mathcal{L}_{data}(\theta) + \alpha \mathcal{L}_{phy}(\theta, \Xi, \pi), \quad (3)$$

where

$$\mathcal{L}_{data} = \frac{1}{nmT} \sum_{x,y,t} \|f_\theta - u\|_2^2, \quad (4)$$

$$\mathcal{L}_{phy} = \frac{1}{n'm'T'} \sum_{x',y',t'} \left\| \frac{\partial f_\theta}{\partial t} - \Phi(f_\theta)\Xi - Q_\pi \right\|_2^2. \quad (5)$$

Here, data loss measures how well $f_\theta$ approximates $u$ well on the weather data, and physical loss measures how well the learned equation fits the weather data. The two regularization losses prevent the overfitting of explicit PDE terms $f_\theta$ and the latent force $Q_\pi$.

## 3.4 Physics-Guided Fine-Tuning for Pre-Trained Weather Forecasting Models

In theory, $f_\theta(x, y, t)$ can also take in future data coordinates and produce the extrapolation directly. However, as $f_\theta(x, y, t)$ is only trained on historical weather data, while anywhere outside the bounds of where the model was trained is completely unknown. Empirically, we find that $f_\theta$ alone does not exhibit strong extrapolation or forecasting performance. To improve the extrapolation ability, instead of using $f_\theta$ directly, we propose to take advantage of the learned physical mechanism represented by $\Xi$ and $Q_\pi$ to improve another forecasting model $g_\omega$, which takes historical spatiotemporal data and predicts the future.

Moreover, once $f_\theta$ is trained, it can generate weather variables at arbitrary spatiotemporal coordinates $(x', y', t)$, enabling flexible control over the resolution of historical data used to train or fine-tune $g_\omega$. This allows seamless integration with any pre-trained forecasting model by aligning spatiotemporal granularity as needed.

The overall framework of weather forecasting is depicted in Fig. 2. To calculate differential terms efficiently, we propose to use finite difference (FD) approximations on super-resolution data from weather downscaling, which is extremely fast, instead of training a
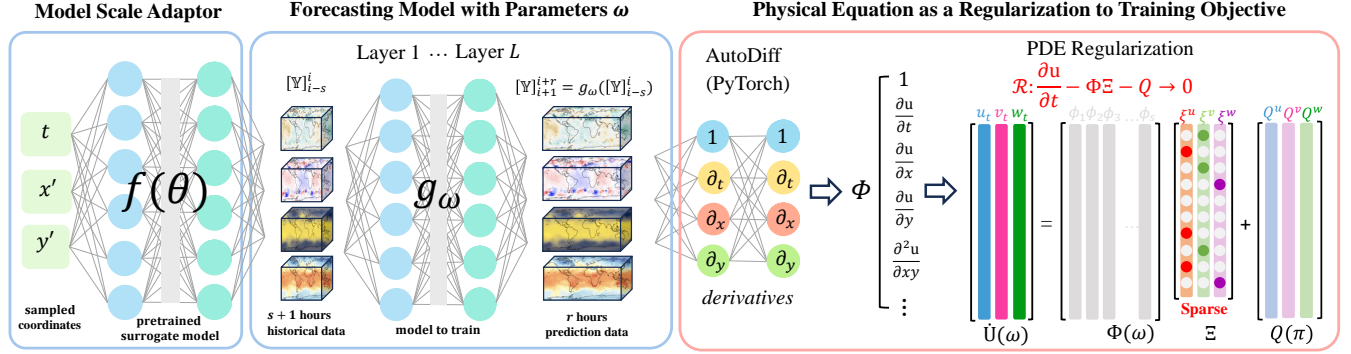
**Figure 2: Schematic diagram of *PhyDL-NWP* for forecasting. We first use pre-trained surrogate model for weather downscaling to perform data augmentation, which is a necessity for aligning weather data resolution in the forecasting model. Then, we take the augmented historical data and use a pre-trained state-of-the-art forecasting model to predict future data. Based on the spatio-temporal coordinates of the predicted data, we add a physics loss to recover the previously learned PDE.**

surrogate model for every time frame $i$. The overall loss function $\mathcal{L}_F$ for weather forecasting is:

$$\mathcal{L}_F(\omega) = \mathcal{L}_{\text{data}}(\omega) + \beta \mathcal{L}_{\text{phy}}(\omega), \tag{6}$$

where

$$\mathcal{L}_{\text{data}}(\omega) = \frac{1}{nmr \cdot q} \sum_{i=s+1}^{T-r} \left\| g_\omega([\mathbb{Y}]_{i-s}^i) - [\mathbb{Y}]_{i+1}^{i+r} \right\|_2^2, \tag{7}$$

$$\mathcal{L}_{\text{phy}}(\omega) = \frac{1}{nmr \cdot q} \sum_{i=s+1}^{T-r} \left\| \frac{\partial g_\omega([\mathbb{Y}]_{i-s}^i)}{\partial t} - p \right\|_2^2, \tag{8}$$

with $q = \text{T-r-s-1}$, $p = \Phi(g_\omega([\mathbb{Y}]_{i-s}^i))\Xi + Q_\pi$. Note that $\theta$, $\Xi$, and $\pi$ are already learned during the downscaling beforehand. $\alpha, \beta, \sigma_1, \sigma_2$ are all hyperparameters to balance the different loss terms. As long as the downscaling model $f_\theta$ is accurate, the recovered physics offers a globally consistent constraint that enhances the generalization of $g_\omega$ without adding substantial model complexity. The size of the parameters as well as the inference speed of the different models are summarized in Table 1. The number of parameters of *PhyDL-NWP* is much smaller than other models, thus it is much faster to perform forward/backward propagation on $f_\theta$ and $g_\omega$.

## 4 Experiments

We conduct both the forecasting and downscaling performance comparisons. All experiments were carried out on four NVIDIA A100 graphical cards. Only the performances on the test sets at the optimal performance on the validation sets are reported. The maximum training epochs are 50. Every result is the average of three independent trainings under different random seeds. We select a few representative weather variables and the average of all in the tables for visualization. The average of all variables reflects the overall performance. We use two commonly used metrics [2] for evaluation: Root Mean Square Error (RMSE) and Anomaly Correlation Coefficient (ACC). For both downscaling and forecasting, we split by 8:1:1 for train/validation/test datasets in chronological order. Code to implement PhyDL-NWP is available in GitHub[3].

[3]https://github.com/yingtaoluo/PhyDL-NWP

### 4.1 Downscaling Performance Comparison

We evaluate the effectiveness of *PhyDL-NWP* and other baseline models for weather downscaling on a real-world dataset Huadong, which is derived from the European Centre for Medium-Range Weather Forecasts (ECMWF) operational forecast (HRES) and re-analysis (ERA5) archive. It comprises a grid of $64 \times 44$ cells, with each cell having a grid size of 0.25 degrees in both latitude and longitude. More data details can be found in Appendix A.1. Since most previous studies on weather downscaling can only handle the downscaling of the two spatial dimensions, for the sake of comparison, we also only report the performance of *PhyDL-NWP* on spatial downscaling in Table 2. We perform 2x and 4x downscaling tasks with 0.5 and 1 degrees resolutions, respectively. To facilitate this, the 0.25-degree HRES data undergoes linear interpolation to generate the requisite 0.5-degree and 1-degree input data. We compare our model against the Bicubic interpolation, FSRCNN [27], Res-DeepD [32], EDSR [10], RCAN [43], YNet [20], DeepSD [35], and GINE [26]. For the deep learning baselines, channel-wise normalization is performed for efficiency. Unlike prior methods that rely on fine-granular labels for supervision, *PhyDL-NWP* learns from coarse-granular inputs alone by aligning with physical principles, enabling it to perform super-resolution without labeled training outputs. Details about baselines can be found in Appendix A.2.4.

From Table 2, we can conclude that *PhyDL-NWP* provides a significant improvement up to 20.1% to 24.6% on average over RMSE against the baseline models. Well-recognized deep learning models like FSRCNN and YNet achieve much worse results, which could be because most models only consider the downscaling of spatial dimensions, neglecting the patterns in the temporal dimension. Moreover, weather data is multivariable, and the spatio-temporal dependencies are complex, making it difficult to recover the ground-truth information without global modeling. Furthermore, we find that the RMSE for 2x and 4x resolutions is close. Since *PhyDL-NWP* can provide infinite resolution results given continuous coordinates, we believe that it will be accurate for higher resolution downscaling, based on this evidence. Moreover, *PhyDL-NWP* can easily perform downscaling in the temporal dimension. We only experiment on spatial dimension to align with existing models.

**Table 1: Comparison of the number of model parameters and running speed for weather forecasting on WeatherBench dataset.** *PhyDL-NWP* **is a light-weighted and efficient plug-and-play module, while others are standalone models.** *PhyDL-NWP* **is about 55~170 times faster and 10~3600 times lighter than a standalone model.**

| Model/Module | **PhyDL-NWP** | BiLSTM | Hybrid-CBA | ConvLSTM | AFNO | MTGNN | MegaCRN | ClimaX | FourcastNet | GraphCast |
|---|---|---|---|---|---|---|---|---|---|---|
| Number of parameters | **55K** | 171M | 198M | 678K | 520K | 1.6M | 580K | 107M | 73M | 36M |
| Time cost per epoch | **7.8s** | 11.9min | 15.6min | 7.1min | 9.4min | 9.9min | 8.5min | 22.2min | 16.5min | 13.6min |

**Table 2: The RMSE comparison of weather downscaling for Huadong dataset. Bold fonts mark the best performances, and underlines mark the second-best performances. The Improv shows the percentage of improvement over the base model, which is statistically significant as measured by t-test with p-value< 0.01.**

| Model | 100m Wind (U) | | 10m Wind (U) | | Temperature | | Surface Pressure | | Average | |
|---|---|---|---|---|---|---|---|---|---|---|
| | 2x | 4x | 2x | 4x | 2x | 4x | 2x | 4x | 2x | 4x |
| Bicubic | 1.687 | 1.765 | 1.215 | 1.272 | 1.714 | 1.848 | 0.818 | 1.220 | 1.515 | 1.654 |
| EDSR | 1.145 | 1.176 | 1.020 | 1.113 | 1.217 | 1.275 | 0.460 | 0.552 | 1.068 | 1.156 |
| ResDeepD | <u>1.092</u> | <u>1.111</u> | 1.003 | 1.079 | 1.182 | <u>1.204</u> | <u>0.301</u> | <u>0.317</u> | <u>1.010</u> | <u>1.043</u> |
| RCAN | 1.169 | 1.199 | <u>0.808</u> | <u>1.038</u> | 1.219 | 1.259 | 0.572 | 0.609 | 1.092 | 1.144 |
| FSRCNN | 1.197 | 1.202 | 1.090 | 1.126 | 1.198 | 1.233 | 0.430 | 0.560 | 1.093 | 1.149 |
| YNet | 1.116 | 1.125 | 0.947 | 1.103 | 1.192 | 1.226 | 0.467 | 0.575 | 1.062 | 1.125 |
| DeepSD | 1.205 | 1.216 | 1.020 | 1.117 | 1.218 | 1.265 | 0.454 | 0.591 | 1.087 | 1.149 |
| GINE | 1.126 | 1.285 | 0.875 | 1.069 | <u>1.166</u> | 1.235 | 0.350 | 0.363 | 1.036 | 1.101 |
| PhyDL-NWP | **0.973** | **0.970** | **0.696** | **0.693** | **0.905** | **0.904** | **0.211** | **0.216** | **0.794** | **0.789** |
| Improv | 10.9% | 12.7% | 13.9% | 33.2% | 22.4% | 24.9% | 29.9% | 31.9% | 20.1% | 24.6% |

**Table 3: Model comparison of seven-day weather forecasting for real-measurement Ningbo dataset. The Improv shows the percentage of improvement over the base model, which is statistically significant as measured by t-test with p-value< 0.01.**

| Model | 100m Wind | | 10m Wind | | Humidity | | Temperature | | Average | |
|---|---|---|---|---|---|---|---|---|---|---|
| | RMSE↓ | ACC↑ | RMSE↓ | ACC↑ | RMSE↓ | ACC↑ | RMSE↓ | ACC↑ | RMSE↓ | ACC↑ |
| NWP | 0.892 | 0.606 | 0.875 | 0.581 | 0.932 | **0.699** | 0.422 | 0.910 | 0.868 | **0.587** |
| PINN | **0.622** | 0.520 | **0.605** | 0.489 | 0.835 | 0.443 | 0.657 | 0.727 | 0.652 | 0.427 |
| PINO | 0.640 | 0.504 | 0.602 | 0.516 | 0.609 | 0.538 | 0.477 | 0.838 | 0.626 | 0.452 |
| Bi-LSTM-T | 0.666 | 0.588 | 0.704 | 0.562 | 0.576 | 0.597 | 0.472 | 0.876 | 0.601 | 0.443 |
| Bi-LSTM-T+ | 0.635 | **0.649** | <u>0.664</u> | <u>0.621</u> | 0.550 | 0.672 | 0.442 | 0.903 | 0.571 | 0.485 |
| Improv | 4.65% | 10.4% | 5.68% | 10.5% | 4.51% | 12.6% | 6.36% | 3.08% | 5.00% | 9.48% |
| Hybrid-CBA | 0.674 | 0.568 | 0.717 | 0.550 | 0.590 | 0.595 | 0.460 | 0.865 | 0.617 | 0.431 |
| Hybrid-CBA+ | 0.641 | 0.637 | 0.680 | 0.609 | 0.572 | 0.657 | 0.411 | 0.906 | 0.586 | 0.474 |
| Improv | 4.90% | 12.1% | 5.16% | 10.7% | 3.05% | 10.4% | 10.7% | 4.74% | 5.02% | 9.98% |
| ConvLSTM | 0.701 | 0.524 | 0.732 | 0.535 | 0.572 | 0.602 | 0.489 | 0.858 | 0.636 | 0.418 |
| ConvLSTM+ | 0.658 | 0.587 | 0.699 | 0.607 | 0.550 | 0.671 | 0.454 | 0.891 | 0.596 | 0.463 |
| Improv | 6.13% | 12.0% | 4.51% | 13.5% | 3.85% | 11.5% | 7.16% | 3.85% | 5.97% | 10.8% |
| AFNO | 0.659 | 0.592 | 0.710 | 0.546 | 0.528 | 0.584 | 0.429 | 0.894 | 0.599 | 0.465 |
| AFNO+ | <u>0.625</u> | <u>0.648</u> | 0.669 | **0.630** | <u>0.500</u> | <u>0.695</u> | <u>0.397</u> | **0.929** | <u>0.556</u> | <u>0.530</u> |
| Improv | 5.16% | 9.46% | 5.78% | 15.4% | 5.30% | 19.0% | 7.46% | 3.91% | 7.18% | 14.0% |
| MTGNN | 0.685 | 0.566 | 0.720 | 0.538 | 0.521 | 0.589 | 0.434 | 0.887 | 0.597 | 0.457 |
| MTGNN+ | 0.657 | 0.629 | 0.672 | 0.613 | **0.489** | 0.679 | **0.388** | <u>0.918</u> | **0.555** | 0.514 |
| Improv | 4.09% | 11.1% | 6.67% | 13.9% | 6.14% | 15.3% | 10.6% | 3.49% | 7.04% | 12.5% |
| MegaCRN | 0.698 | 0.520 | 0.734 | 0.535 | 0.544 | 0.595 | 0.492 | 0.866 | 0.621 | 0.426 |
| MegaCRN+ | 0.667 | 0.591 | 0.684 | 0.600 | 0.521 | 0.666 | 0.458 | 0.907 | 0.590 | 0.477 |
| Improv | 4.44% | 13.7% | 6.81% | 12.1% | 4.23% | 11.9% | 6.91% | 4.73% | 5.00% | 12.0% |

## 4.2 Forecasting Performance Comparison

We evaluate the effectiveness of *PhyDL-NWP* for weather forecasting on two real-world reanalysis datasets derived from ERA5[4]: Ningxia and WeatherBench[5]. In addition to reanalysis data, we also test on a more accurate real-world measurement (observational) dataset Ningbo, where meteorological factors are directly collected from the Ningbo Meteorological Bureau[6]. Ningbo and Ningxia cover two different terrains and climate types in 0.25 degrees resolution, while WeatherBench covers the global weather in 5.625 degrees
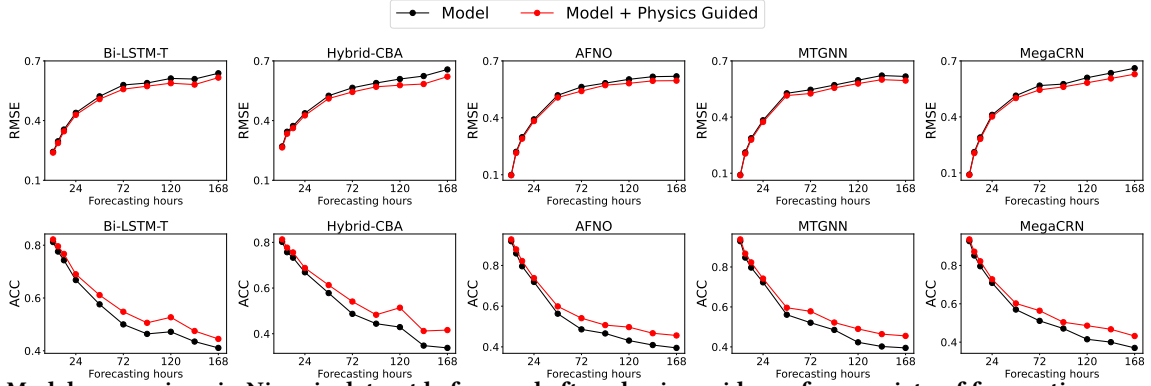
---

**Figure 3: Model comparison in Ningxia dataset before and after physics guidance for a variety of forecasting ranges on the average of all weather variables.**

resolution. On each grid in both datasets, we select the most important observational weather information for evaluation. See more details in Appendix A.1. We perform multiple experiments based on the length of future prediction, ranging from one hour to seven days. Due to the GPU memory limitation, we use the eight weather variables of only ten hours in the past to predict all eight weather variables in the future.

There are five kinds of baseline models in comparison, including: (1) Physics-based models: NWP, PINN [30], PINO [17]; (2) Meteorological models: Bi-LSTM-T [42], Hybrid-CBA [7]; (3) Vision models: ConvLSTM [33], FourcastNet [28] based on AFNO [5], ClimaX [24]; (4) Spatio-temporal graph models: MTGNN [40], MegaCRN [11], GraphCast [14]. Some baseline models are slightly modified to adapt to the multi-step prediction setting and/or specific modeling resolution, with details described in the Appendix A.2.4. Besides deep learning models, we also compare these models with the Numerical Weather Prediction (NWP) results provided by ECMWF IFS and the Physical-Informed Neural Network (PINN) [30] based on the PDEs learned by *PhyDL-NWP*. We denote the baseline models as **BaseModels** and incorporate them with *PhyDL-NWP* as **BaseModels+**.

*4.2.1 Regional Weather Forecasting.* In particular, the result of regional forecasting details with seven days are reported in Table 3 in the main manuscript and Table 5 in the appendix, as it represents the model's capability of long-term medium-range regional weather prediction. The vanilla PINN does not seem to be effective, while the improvement provided by *PhyDL-NWP* is consistently significant. For Ningbo dataset, the overall improvement on the average of all weather variables is up to **7.18% over RMSE** and **14.0% over ACC**; for Ningxia dataset, the overall improvement on that is up to **5.48% over RMSE** and **18.8% over ACC**. All the results are **statistically significant**. Furthermore, we find that NWP is good in ACC, while being the worst in RMSE. Deep learning models, on the other hand, greatly outperform NWP in RMSE, showing great advantage in modeling capacity.

To understand the holistic properties of *PhyDL-NWP*, we conduct detailed analyses on the Ningxia dataset. First, the comparison of different models for different forecasting ranges is visualized in Fig. 3. **BaseModels+** excels **BaseModels** and NWP at all time steps. As the forecasting range increases, the deep learning performance

decreases quickly. The improvement provided by *PhyDL-NWP*, however, is increasing in the forecasting range, which highlights its unique advantages of guiding models for long-term forecasting.

In addition, based on AFNO from FourcastNet, we visualize its forecasting comparison at the 10-th time frame in Fig. 4. *PhyDL-NWP* clearly improves the performance of the existing deep model, making the forecasting results closer to the ground truth. Specifically, "Total precipitation" is not a typical physical quantity and is hard to predict due to lack of effective physical equation. While the vanilla AFNO is a total disaster, AFNO+ provides information about which local areas receive concentrated rainfall. This effectively demonstrated the success of our implemented parameterization strategy with the latent force model.

*4.2.2 Global Weather Forecasting.* Besides regional weather forecasting, we also test *PhyDL-NWP* on the global weather forecasting task, which is the benchmark for a lot of recent works. The results with WeatherBench dataset for global weather forecasting are reported in Table 4. In comparison, *PhyDL-NWP* shows a lot more improvements over baseline models in the coarser-granular WeatherBench dataset, with **statistically significant improvement over RMSE**. It is also worth noting that, even for the state-of-the-art GraphCast model, there is still an improvement. Moreover, as reported in Table 1, *PhyDL-NWP* module is extremely light-weighted and efficient, with a time cost that is **55~170 times faster** than the base forecasting models. The integration of physics and deep learning is clearly demonstrated in this study.

## 4.3 Meteorology Dynamics Interpretation

To understand how *PhyDL-NWP* is grounded on laws of physics, we compare the learned dynamics by *PhyDL-NWP* from Huadong dataset with the basic equations of NWP [34]. These equations originate from conservation of mass, energy, and momentum. *PhyDL-NWP* will explicitly use the terms that appear in the first-principle equations and can be represented based on the dataset, while modeling the rest of the dynamics using latent force parameterization. As shown in Table 6, our latent parameterization strategy is proposed considering that many terms cannot be modeled explicitly, due to missing records in the data or difficulty to measure.

**Table 4: Model comparison of global weather forecasting up to two days for the WeatherBench dataset. All the reported results are averaged after three runs. BaseModel+ denotes the original model with *PhyDL-NWP* module.**

| Variable | Hours | ClimaX | | ClimaX+ | | FourcastNet | | FourcastNet+ | | GraphCast | | GraphCast+ | |
|---|---|---|---|---|---|---|---|---|---|---|---|---|---|
| | | RMSE↓ | ACC↑ | RMSE↓ | ACC↑ | RMSE↓ | ACC↑ | RMSE↓ | ACC↑ | RMSE↓ | ACC↑ | RMSE↓ | ACC↑ |
| t2m | 6 | 1.46 | 0.92 | 1.13 | 0.98 | 1.27 | 0.99 | 1.01 | 0.99 | 0.40 | 0.99 | 0.39 | 0.99 |
| | 12 | 1.58 | 0.91 | 1.25 | 0.96 | 1.48 | 0.98 | 1.12 | 0.99 | 0.47 | 0.99 | 0.46 | 0.99 |
| | 18 | 1.75 | 0.90 | 1.42 | 0.95 | 1.63 | 0.98 | 1.27 | 0.99 | 0.52 | 0.99 | 0.50 | 0.99 |
| | 24 | 1.90 | 0.88 | 1.58 | 0.94 | 1.69 | 0.96 | 1.40 | 0.98 | 0.59 | 0.99 | 0.56 | 0.99 |
| | 48 | 2.80 | 0.84 | 2.34 | 0.92 | 2.26 | 0.94 | 1.90 | 0.97 | 0.74 | 0.98 | 0.72 | 0.99 |
| t | 6 | 1.32 | 0.95 | 1.02 | 0.98 | 1.15 | 0.99 | 0.99 | 0.99 | 0.39 | 0.99 | 0.39 | 0.99 |
| | 12 | 1.66 | 0.94 | 1.28 | 0.98 | 1.36 | 0.99 | 1.17 | 0.99 | 0.46 | 0.99 | 0.45 | 0.99 |
| | 18 | 1.87 | 0.92 | 1.48 | 0.97 | 1.53 | 0.99 | 1.35 | 0.99 | 0.53 | 0.99 | 0.51 | 0.99 |
| | 24 | 2.16 | 0.91 | 1.66 | 0.96 | 1.66 | 0.98 | 1.52 | 0.99 | 0.59 | 0.99 | 0.57 | 0.99 |
| | 48 | 2.94 | 0.86 | 2.11 | 0.95 | 1.94 | 0.97 | 1.70 | 0.99 | 0.80 | 0.99 | 0.77 | 0.99 |
| z | 6 | 207.6 | 0.93 | 128.5 | 0.97 | 142.3 | 0.96 | 100.8 | 0.99 | 44.1 | 0.99 | 44.0 | 0.99 |
| | 12 | 222.3 | 0.90 | 159.9 | 0.96 | 217.2 | 0.89 | 126.6 | 0.99 | 47.6 | 0.99 | 47.2 | 0.99 |
| | 18 | 268.7 | 0.87 | 197.6 | 0.95 | 255.0 | 0.74 | 166.2 | 0.98 | 50.6 | 0.99 | 49.5 | 0.99 |
| | 24 | 305.5 | 0.84 | 224.1 | 0.94 | 304.2 | 0.71 | 203.2 | 0.97 | 78.4 | 0.98 | 75.7 | 0.99 |
| | 48 | 497.2 | 0.77 | 292.4 | 0.92 | 477.6 | 0.62 | 278.0 | 0.95 | 118.6 | 0.98 | 112.5 | 0.98 |
| u10 | 6 | 1.56 | 0.90 | 1.28 | 0.94 | 1.39 | 0.93 | 1.12 | 0.95 | 0.50 | 0.98 | 0.50 | 0.98 |
| | 12 | 1.98 | 0.89 | 1.73 | 0.94 | 1.88 | 0.92 | 1.69 | 0.94 | 0.53 | 0.98 | 0.53 | 0.98 |
| | 18 | 2.20 | 0.89 | 1.94 | 0.93 | 2.10 | 0.90 | 1.88 | 0.93 | 0.57 | 0.98 | 0.56 | 0.98 |
| | 24 | 2.46 | 0.85 | 2.15 | 0.92 | 2.36 | 0.89 | 2.09 | 0.92 | 0.75 | 0.97 | 0.73 | 0.98 |
| | 48 | 2.91 | 0.78 | 2.46 | 0.88 | 2.79 | 0.88 | 2.36 | 0.90 | 1.24 | 0.96 | 1.16 | 0.97 |
| v10 | 6 | 1.78 | 0.88 | 1.37 | 0.94 | 1.55 | 0.94 | 1.22 | 0.94 | 0.52 | 0.98 | 0.52 | 0.98 |
| | 12 | 1.99 | 0.86 | 1.52 | 0.93 | 1.81 | 0.90 | 1.39 | 0.93 | 0.55 | 0.98 | 0.55 | 0.98 |
| | 18 | 2.35 | 0.85 | 1.74 | 0.92 | 2.11 | 0.88 | 1.63 | 0.92 | 0.58 | 0.98 | 0.57 | 0.98 |
| | 24 | 2.66 | 0.83 | 2.08 | 0.90 | 2.40 | 0.85 | 1.96 | 0.91 | 0.79 | 0.97 | 0.76 | 0.98 |
| | 48 | 3.74 | 0.70 | 2.49 | 0.87 | 3.06 | 0.80 | 2.25 | 0.89 | 1.36 | 0.96 | 1.24 | 0.97 |

**Table 5: Model comparison of seven-day medium-range weather forecasting for Ningxia dataset.**

| Model | 100m Wind(U) | | 10m Wind(U) | | Temperature | | Surface pressure | | Average | |
|---|---|---|---|---|---|---|---|---|---|---|
| | RMSE↓ | ACC↑ | RMSE↓ | ACC↑ | RMSE↓ | ACC↑ | RMSE↓ | ACC↑ | RMSE↓ | ACC↑ |
| NWP | 0.968 | 0.521 | 0.933 | 0.514 | **0.319** | **0.844** | 0.325 | 0.961 | 0.901 | **0.526** |
| PINN | **0.697** | 0.470 | **0.681** | 0.437 | 0.635 | 0.654 | 0.494 | 0.904 | 0.666 | 0.387 |
| Bi-LSTM-T | 0.822 | 0.502 | 0.804 | 0.485 | 0.583 | 0.525 | 0.160 | 0.961 | 0.638 | 0.411 |
| Bi-LSTM-T+ | <u>0.798</u> | **0.545** | <u>0.777</u> | <u>0.520</u> | 0.560 | 0.584 | 0.156 | <u>0.965</u> | 0.616 | 0.445 |
| Improv | 2.92% | 8.57% | 3.36% | 7.22% | 4.28% | 11.2% | 2.50% | 0.42% | 3.45% | 8.27% |
| Hybrid-CBA | 0.842 | 0.456 | 0.819 | 0.445 | 0.652 | 0.430 | <u>0.150</u> | 0.964 | 0.657 | 0.338 |
| Hybrid-CBA+ | 0.801 | <u>0.536</u> | 0.790 | 0.509 | 0.563 | 0.589 | **0.149** | **0.966** | 0.621 | 0.416 |
| Improv | 4.87% | 17.5% | 3.54% | 14.4% | 13.7% | 37.0% | 0.67% | 0.21% | 5.48% | 18.8% |
| ConvLSTM | 0.865 | 0.429 | 0.848 | 0.408 | 0.592 | 0.499 | 0.175 | 0.959 | 0.656 | 0.364 |
| ConvLSTM+ | 0.826 | 0.477 | 0.814 | 0.472 | 0.520 | 0.619 | 0.170 | 0.955 | 0.622 | 0.419 |
| Improv | 4.51% | 11.2% | 4.01% | 15.7% | 12.2% | 24.0% | 2.86% | -0.42% | 5.18% | 15.1% |
| AFNO | 0.856 | 0.436 | 0.838 | 0.421 | 0.501 | 0.571 | 0.153 | 0.962 | 0.619 | 0.395 |
| AFNO+ | 0.823 | 0.505 | 0.808 | 0.498 | <u>0.466</u> | 0.693 | 0.153 | 0.956 | <u>0.596</u> | <u>0.456</u> |
| Improv | 3.86% | 15.8% | 3.58% | 18.3% | 6.99% | 17.9% | 0.00% | -0.31% | 3.72% | 15.4% |
| MTGNN | 0.835 | 0.484 | 0.820 | 0.465 | 0.502 | 0.526 | 0.162 | 0.958 | 0.617 | 0.395 |
| MTGNN+ | 0.810 | 0.525 | 0.792 | **0.521** | 0.469 | <u>0.677</u> | 0.160 | 0.959 | **0.595** | 0.455 |
| Improv | 2.99% | 8.47% | 3.41% | 12.0% | 6.57% | 28.7% | 1.96% | 0.10% | 3.57% | 15.2% |
| MegaCRN | 0.840 | 0.455 | 0.824 | 0.432 | 0.646 | 0.487 | 0.188 | 0.958 | 0.661 | 0.370 |
| MegaCRN+ | 0.809 | 0.510 | 0.793 | 0.485 | 0.598 | 0.600 | 0.183 | 0.954 | 0.629 | 0.432 |
| Improv | 4.64% | 12.1% | 3.76% | 12.3% | 7.43% | 23.2% | 2.66% | -0.42% | 4.84% | 16.8% |

For the modeling of temperature, the basic equation originates from the 3D convection-diffusion equation for heat transfer. Temperature $T$ is influenced by advection (movement of heat due to fluid flow, represented by the velocity components $U$, $V$ and a vertical component $W$ along height $z$), diffusion (spread of heat due to thermal diffusivity $k$), and a heat source $H$. In addition, $t$ denotes time, $x$ and $y$ denote space, $U_{10}$ represents the wind components at the heights of 10m. An example of meteorology dynamics of temperature (t) of WeatherBench dataset in the year of 2018 is shown in Fig. 5. We found that $Q$ and $\Phi\Xi$ substitute each other well and the combination generally matches $\frac{\partial T}{\partial t}$.
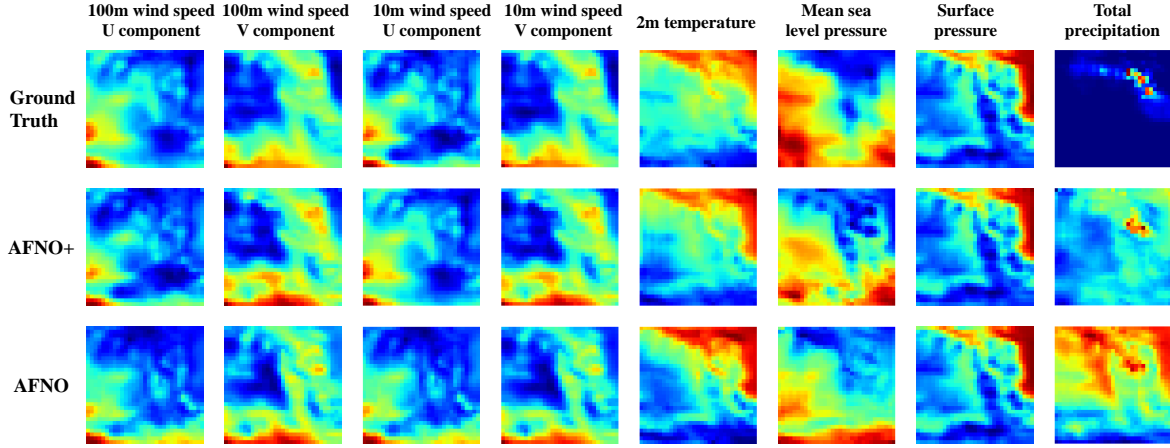
| | 100m wind speed U component | 100m wind speed V component | 10m wind speed U component | 10m wind speed V component | 2m temperature | Mean sea level pressure | Surface pressure | Total precipitation |
|---|---|---|---|---|---|---|---|---|
| Ground Truth | | | | | | | | |
| AFNO+ | | | | | | | | |
| AFNO | | | | | | | | |

**Figure 4: Example of comparison of 7-day weather forecast results in Ningxia dataset. AFNO+ are closer to the ground truth.**

**Table 6: Comparison of learned dynamics against ground truth in literature. Orange color marks terms unavailable from the data, which are represented by latent force $Q$.**

| Temperature | Learned vs. True PDE |
|---|---|
| Learned | $\frac{\partial T}{\partial t} = -U_{10}\frac{\partial T}{\partial x} - V_{10}\frac{\partial T}{\partial y} + Q$ |
| Ground Truth | $\frac{\partial T}{\partial t} = -U\frac{\partial T}{\partial x} - V\frac{\partial T}{\partial y} - W\frac{\partial T}{\partial z} + k\frac{\partial^2 T}{\partial z^2} + H$ |
| **Wind Velocity** | **Learned vs. True PDE** |
| Learned | $\frac{\partial U_{10}}{\partial t} = -U_{10}\frac{\partial U_{10}}{\partial x} - V_{10}\frac{\partial U_{10}}{\partial y} + Q$ |
| Ground Truth | $\frac{\partial U}{\partial t} = -U\frac{\partial U}{\partial x} - V\frac{\partial U}{\partial y} - W\frac{\partial U}{\partial z} - \frac{1}{\rho}\frac{\partial p}{\partial x} + \nu\Delta\mathbf{u} + F_{f_x}$ |
| **Surface Pressure** | **Learned vs. True PDE** |
| Learned | $\frac{\partial^2 p}{\partial t^2} = \frac{\partial^2 p}{\partial x^2} + \frac{\partial^2 p}{\partial y^2} + Q$ |
| Ground Truth | $\frac{\partial^2 p}{\partial t^2} = \frac{\partial^2 p}{\partial x^2} + \frac{\partial^2 p}{\partial y^2} + \frac{\partial^2 p}{\partial z^2}$ |
| **Humidity** | **Learned vs. True PDE** |
| Learned | $\frac{\partial q}{\partial t} = -U\frac{\partial q}{\partial x} - V\frac{\partial q}{\partial y} + \frac{\partial^2 q}{\partial x^2} + \frac{\partial^2 q}{\partial y^2} + Q$ |
| Ground Truth | $\frac{\partial q}{\partial t} = -U\frac{\partial q}{\partial x} - V\frac{\partial q}{\partial y} - W\frac{\partial q}{\partial z} + k\nabla^2 q + S_q$ |



**Figure 5: The latent force and PDE for the temperature variation in WeatherBench dataset.**

For wind velocity, the compared basic equation originates from the 3D Navier-Stokes equations. The velocity is influenced by convective acceleration, the gradient of pressure $p$ with fluid density $\rho$, the diffusion of momentum due to viscosity $\nu$ for velocity of all directions $\mathbf{u}$, and external force $F_{f_x}$ along the $x$ direction (such as friction). It is obvious that the WeatherBench dataset does not provide all the necessary variables to complete the equation. Our latent force model will address this problem well. Similarly, for surface pressure, the learned equation aligns with the 3D wave equation while the missing vertical component is for the latent force $Q$ to capture. For humidity, the equation originates from the conservation of mass, and combines the advection, diffusion and source terms, where $q$ is the humidity, and $S_q$ is the source term for humidity (e.g., evaporation, condensation). We approximate precipitation using a parameterized PDE for humidity as a tractable surrogate that captures its dominant drivers.
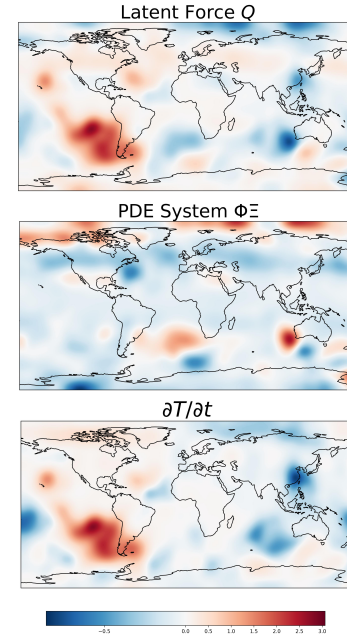
## 5  Conclusion

We introduce *PhyDL-NWP*, a light-weighted physics-guided deep learning framework for weather downscaling and forecasting. By incorporating parameterized physical dynamics through latent force modeling, *PhyDL-NWP* enables continuous, resolution-free predictions while ensuring consistency with governing equations. It can augment and fine-tune existing forecasting models with minimal overhead, significantly improving both accuracy and physical plausibility. Extensive experiments across diverse datasets demonstrate its effectiveness, scalability, and interpretability, positioning *PhyDL-NWP* as a practical and generalizable module for modern meteorological modeling.

# References

[1] Peter Bauer, Alan Thorpe, and Gilbert Brunet. 2015. The quiet revolution of numerical weather prediction. *Nature* 525, 7567 (2015), 47–55.

[2] Kaifeng Bi, Lingxi Xie, Hengheng Zhang, Xin Chen, Xiaotao Gu, and Qi Tian. 2023. Accurate medium-range global weather forecasting with 3D neural networks. *Nature* (2023), 1–6.

[3] Kang Chen, Tao Han, Junchao Gong, Lei Bai, Fenghua Ling, Jing-Jia Luo, Xi Chen, Leiming Ma, Tianning Zhang, Rui Su, et al. 2023. FengWu: Pushing the Skillful Global Medium-range Weather Forecast beyond 10 Days Lead. *arXiv preprint arXiv:2304.02948* (2023).

[4] Yuntian Chen, Yingtao Luo, Qiang Liu, Hao Xu, and Dongxiao Zhang. 2022. Symbolic genetic algorithm for discovering open-form partial differential equations (SGA-PDE). *Physical Review Research* 4, 2 (2022), 023174.

[5] John Guibas, Morteza Mardani, Zongyi Li, Andrew Tao, Anima Anandkumar, and Bryan Catanzaro. 2021. Adaptive fourier neural operators: Efficient token mixers for transformers. *arXiv preprint arXiv:2111.13587* (2021).

[6] Jindong Han, Hao Liu, Hengshu Zhu, Hui Xiong, and Dejing Dou. 2021. Joint air quality and weather prediction based on multi-adversarial spatiotemporal networks. In *Proceedings of the AAAI Conference on Artificial Intelligence*, Vol. 35. 4081–4089.

[7] Yan Han, Lihua Mi, Lian Shen, CS Cai, Yuchen Liu, Kai Li, and Guoji Xu. 2022. A short-term wind speed prediction method utilizing novel hybrid deep learning algorithms to correct numerical weather forecasting. *Applied Energy* 312 (2022), 118777.

[8] Hans Hersbach, Bill Bell, Paul Berrisford, Shoji Hirahara, András Horányi, Joaquín Muñoz-Sabater, Julien Nicolas, Carole Peubey, Raluca Radu, Dinand Schepers, et al. 2020. The ERA5 global reanalysis. *Quarterly Journal of the Royal Meteorological Society* 146, 730 (2020), 1999–2049.

[9] Shuai Hu, Yue Xiang, Da Huo, Shafqat Jawad, and Junyong Liu. 2021. An improved deep belief network based hybrid forecasting method for wind power. *Energy* 224 (2021), 120185.

[10] Hao Jiang and Li Chen. 2022. An Efficient Content-aware Downsampling-based Video Compression Framework. In *2022 IEEE International Conference on Visual Communications and Image Processing (VCIP)*. IEEE, 1–5.

[11] Renhe Jiang, Zhaonan Wang, Jiawei Yong, Puneet Jeph, Quanjun Chen, Yasumasa Kobayashi, Xuan Song, Shintaro Fukushima, and Toyotaro Suzumura. 2023. Spatio-temporal meta-graph learning for traffic forecasting. In *Proceedings of the AAAI Conference on Artificial Intelligence*, Vol. 37. 8078–8086.

[12] George Em Karniadakis, Ioannis G Kevrekidis, Lu Lu, Paris Perdikaris, Sifan Wang, and Liu Yang. 2021. Physics-informed machine learning. *Nature Reviews Physics* 3, 6 (2021), 422–440.

[13] Dmitrii Kochkov, Janni Yuval, Ian Langmore, Peter Norgaard, Jamie Smith, Griffin Mooers, Milan Klöwer, James Lottes, Stephan Rasp, Peter Düben, et al. 2024. Neural general circulation models for weather and climate. *Nature* (2024), 1–7.

[14] Remi Lam, Alvaro Sanchez-Gonzalez, Matthew Willson, Peter Wirnsberger, Meire Fortunato, Alexander Pritzel, Suman Ravuri, Timo Ewalds, Ferran Alet, Zach Eaton-Rosen, et al. 2022. GraphCast: Learning skillful medium-range global weather forecasting. *arXiv preprint arXiv:2212.12794* (2022).

[15] Yu Li, Fei Tang, Xin Gao, Tongyan Zhang, Junfeng Qi, Jiarui Xie, Xinang Li, and Yuhan Guo. 2022. Numerical weather prediction correction strategy for short-term wind power forecasting based on bidirectional gated recurrent unit and XGBoost. *Frontiers in Energy Research* 9 (2022), 836144.

[16] Zongyi Li, Nikola Kovachki, Kamyar Azizzadenesheli, Burigede Liu, Kaushik Bhattacharya, Andrew Stuart, and Anima Anandkumar. 2020. Fourier neural operator for parametric partial differential equations. *arXiv preprint arXiv:2010.08895* (2020).

[17] Zongyi Li, Hongkai Zheng, Nikola Kovachki, David Jin, Haoxuan Chen, Burigede Liu, Kamyar Azizzadenesheli, and Anima Anandkumar. 2024. Physics-informed neural operator for learning partial differential equations. *ACM/JMS Journal of Data Science* 1, 3 (2024), 1–27.

[18] Yuxuan Liang, Haomin Wen, Yutong Xia, Ming Jin, Bin Yang, Flora Salim, Qingsong Wen, Shirui Pan, and Gao Cong. 2025. Foundation Models for Spatio-Temporal Data Science: A Tutorial and Survey. *arXiv preprint arXiv:2503.13502* (2025).

[19] Haitao Lin, Zhangyang Gao, Yongjie Xu, Lirong Wu, Ling Li, and Stan Z Li. 2022. Conditional local convolution for spatio-temporal meteorological forecasting. In *Proceedings of the AAAI Conference on Artificial Intelligence*, Vol. 36. 7470–7478.

[20] Yumin Liu, Auroop R Ganguly, and Jennifer Dy. 2020. Climate downscaling using YNet: A deep convolutional network with skip connections and fusion. In *Proceedings of the 26th ACM SIGKDD International Conference on Knowledge Discovery & Data Mining*. 3145–3153.

[21] Andrew C Lorenc. 1986. Analysis methods for numerical weather prediction. *Quarterly Journal of the Royal Meteorological Society* 112, 474 (1986), 1177–1194.

[22] Yingtao Luo, Qiang Liu, Yuntian Chen, Wenbo Hu, Tian Tian, and Jun Zhu. 2023. Physics-guided discovery of highly nonlinear parametric partial differential equations. In *Proceedings of the 29th ACM SIGKDD Conference on Knowledge Discovery and Data Mining*. 1595–1607.

[23] Yingtao Luo, Chang Xu, Yang Liu, Weiqing Liu, Shun Zheng, and Jiang Bian. 2022. Learning differential operators for interpretable time series modeling. In *Proceedings of the 28th ACM SIGKDD Conference on Knowledge Discovery and Data Mining*. 1192–1201.

[24] Tung Nguyen, Johannes Brandstetter, Ashish Kapoor, Jayesh K Gupta, and Aditya Grover. 2023. ClimaX: A foundation model for weather and climate. *arXiv preprint arXiv:2301.10343* (2023).

[25] Tung Nguyen, Jason Jewik, Hritik Bansal, Prakhar Sharma, and Aditya Grover. 2023. ClimateLearn: Benchmarking Machine Learning for Weather and Climate Modeling. *arXiv preprint arXiv:2307.01909* (2023).

[26] Sungwon Park, Karandeep Singh, Arjun Nellikkattil, Elke Zeller, Tung Duong Mai, and Meeyoung Cha. 2022. Downscaling earth system models with deep learning. In *Proceedings of the 28th ACM SIGKDD conference on knowledge discovery and data mining*. 3733–3742.

[27] Linsey S Passarella, Salil Mahajan, Anikesh Pal, and Matthew R Norman. 2022. Reconstructing high resolution ESM data through a novel fast super resolution convolutional neural network (FSRCNN). *Geophysical Research Letters* 49, 4 (2022), e2021GL097571.

[28] Jaideep Pathak, Shashank Subramanian, Peter Harrington, Sanjeev Raja, Ashesh Chattopadhyay, Morteza Mardani, Thorsten Kurth, David Hall, Zongyi Li, Kamyar Azizzadenesheli, et al. 2022. Fourcastnet: A global data-driven high-resolution weather model using adaptive fourier neural operators. *arXiv preprint arXiv:2202.11214* (2022).

[29] Ilan Price, Alvaro Sanchez-Gonzalez, Ferran Alet, Tom R Andersson, Andrew El-Kadi, Dominic Masters, Timo Ewalds, Jacklynn Stott, Shakir Mohamed, Peter Battaglia, et al. 2023. Gencast: Diffusion-based ensemble forecasting for medium-range weather. *arXiv preprint arXiv:2312.15796* (2023).

[30] Maziar Raissi, Paris Perdikaris, and George E Karniadakis. 2019. Physics-informed neural networks: A deep learning framework for solving forward and inverse problems involving nonlinear partial differential equations. *J. Comput. Phys.* 378 (2019), 686–707.

[31] Stephan Rasp, Peter D Dueben, Sebastian Scher, Jonathan A Weyn, Soukayna Mouatadid, and Nils Thuerey. 2020. WeatherBench: a benchmark data set for data-driven weather forecasting. *Journal of Advances in Modeling Earth Systems* 12, 11 (2020), e2020MS002203.

[32] Sumanta Chandra Mishra Sharma and Adway Mitra. 2022. ResDeepD: A residual super-resolution network for deep downscaling of daily precipitation over India. *Environmental Data Science* 1 (2022), e19.

[33] Xingjian Shi, Zhourong Chen, Hao Wang, Dit-Yan Yeung, Wai-Kin Wong, and Wang-chun Woo. 2015. Convolutional LSTM network: A machine learning approach for precipitation nowcasting. *Advances in neural information processing systems* 28 (2015).

[34] Roland B Stull. 1988. *An introduction to boundary layer meteorology*. Vol. 13. Springer Science & Business Media.

[35] Thomas Vandal, Evan Kodra, Sangram Ganguly, Andrew Michaelis, Ramakrishna Nemani, and Auroop R Ganguly. 2017. Deepsd: Generating high resolution climate change projections through single image super-resolution. In *Proceedings of the 23rd acm sigkdd international conference on knowledge discovery and data mining*. 1663–1672.

[36] Yogesh Verma, Markus Heinonen, and Vikas Garg. 2023. ClimODE: Climate and Weather Forecasting with Physics-informed Neural ODEs. In *The Twelfth International Conference on Learning Representations*.

[37] Bin Wang, Jie Lu, Zheng Yan, Huaishao Luo, Tianrui Li, Yu Zheng, and Guangquan Zhang. 2019. Deep uncertainty quantification: A machine learning approach for weather forecasting. In *Proceedings of the 25th ACM SIGKDD International Conference on Knowledge Discovery & Data Mining*. 2087–2095.

[38] Jonathan A Weyn, Dale R Durran, and Rich Caruana. 2020. Improving data-driven global weather prediction using deep convolutional neural networks on a cubed sphere. *Journal of Advances in Modeling Earth Systems* 12, 9 (2020), e2020MS002109.

[39] Haixu Wu, Hang Zhou, Mingsheng Long, and Jianmin Wang. 2023. Interpretable weather forecasting for worldwide stations with a unified deep model. *Nature Machine Intelligence* (2023), 1–10.

[40] Zonghan Wu, Shirui Pan, Guodong Long, Jing Jiang, Xiaojun Chang, and Chengqi Zhang. 2020. Connecting the dots: Multivariate time series forecasting with graph neural networks. In *Proceedings of the 26th ACM SIGKDD international conference on knowledge discovery & data mining*. 753–763.

[41] Wanghan Xu, Fenghua Ling, Wenlong Zhang, Tao Han, Hao Chen, Wanli Ouyang, and Lei Bai. 2024. Generalizing Weather Forecast to Fine-grained Temporal Scales via Physics-AI Hybrid Modeling. *arXiv preprint arXiv:2405.13796* (2024).

[42] Xiaoying Yang, Shuai Yang, Mou Leong Tan, Hengyang Pan, Hongliang Zhang, Guoqing Wang, Ruimin He, and Zimeng Wang. 2022. Correcting the bias of daily satellite precipitation estimates in tropical regions using deep neural network. *Journal of Hydrology* 608 (2022), 127656.

[43] Tingzhao Yu, Qiuming Kuang, Jiangping Zheng, and Junnan Hu. 2021. Deep precipitation downscaling. *IEEE Geoscience and Remote Sensing Letters* 19 (2021), 1–5.

# A Appendix

## A.1 Dataset Description

---

**Algorithm 1** Physics-Guided Learning of Numerical Weather Prediction (PhyDL-NWP).

---

**Require** Weather data u = $[u_1(x, y, t), \ldots, u_h(x, y, t)]$ with $h$ variables, where $x \in \mathbb{R}^n, y \in \mathbb{R}^m, t \in \mathbb{R}^T$. Alternatively, $T = s + 1$ and $u = [\mathbb{X}]_{i-s}^i \in \mathbb{R}^{n \times m \times h \times (s+1)}$.

**Require** Candidate terms $\Phi(u) = \{\phi_1(u), \ldots, \phi_p(u)\}$ and corresponding coefficients $\Xi = \{\xi_1, \ldots, \xi_p\}$; the latent force model $Q_\pi(x, y, t)$ parameterized by $\pi$; the dynamics model $f_\theta(x, y, t)$ parameterized by $\theta$; pretrained weather forecasting model $g_\omega$ parameterized by $\omega$.

**while** not convergence **do**

    Optimize $\theta$, $\Xi$ and $\pi$ following Eqs. (1-5);

**end while**

Generate super-resolution weather data by downscaling using $\mathbb{Y} = f_\theta(x', y', t)$, where $x' \in \mathbb{R}^{n'}, y' \in \mathbb{R}^{m'}$ are the coordinates of the super-resolution data with $n' > n, m' > m$, which are interpolations within the boundary of where the coordinates of $u$ are located;

**while** not convergence **do**

    Replace $[\mathbb{X}]_{i-s}^i$ by the augmented downscale data $\mathbb{Y}$ and optimize $\omega$ following Eqs. (6-8);

**end while**

**Return** The well-trained weather forecasting model $g_\omega$.

---

For weather downscaling, the Huadong dataset consists of HRES and ERAs datasets. HRES represents a 10-day atmospheric model forecast, while ERA5 serves as a global atmospheric reanalysis, incorporating climate and weather observations. For regional downscaling, we construct a real-world dataset called "Huadong", covering the east China land and sea areas. In this dataset, HRES data is employed as the predictive data, while ERA5 reanalysis data serves as the ground truth.

**Huadong dataset**: The Huadong dataset encompasses a latitude range from $26.8°N$ to $42.9°N$ and a longitude range from $112.6°E$ to $123.7°E$. It comprises a grid of $64 \times 44$ cells, with each cell having a grid size of 0.25 degrees in both latitude and longitude. Notably, the Huadong dataset also incorporates Digital Elevation Model (DEM) data to represent terrain information. Since the terrain information usually refers to the boundary layers in the meteorology model instead of an individual weather factor in the PDE, for simplicity, we do not use this information in the paper. The HRES and ERA5 data cover the period from January 3, 2020, to April 1, 2022. The scores of the average of variables reported in Table 2 are computed based on all eight factors. Due to space limits, we only report the specific scores for four factors.

For weather forecasting, both Ningbo and Ningxia datasets consist of two main components: geographic data and meteorological data. The geographic data includes latitude, longitude, and DEM (Digital Elevation Model) information. The DEM information is commonly used in geographic information systems to represent the terrain of the area. On the other hand, the meteorological data in these datasets consist of various weather factors. These factors typically include wind speed, temperature, and pressure. These data provide information about the atmospheric conditions at different locations within the study area. To organize and represent the data, a grid format is used. In this format, the study area is divided into grids, and each grid cell represents a specific location. Within each grid cell, both the geographic and meteorological data for that location are stored.

**Ningbo dataset**: The Ningbo dataset represents a coastal area spanning from latitude 28.85°N to 30.56°N and longitude 120.91°E to 122.29°E. It is divided into a grid system comprising 58 grids in the latitude direction and 47 in the longitude direction. Each grid has a size of 0.03 degrees in both latitude and longitude. The DEM data are collected from ETOPO1[7]. The meteorological data are collected from Ningbo Meteorological Bureau[8], including 10 weather factors from 1/Jan/2021 to 1/Apr/2021 with 1-hour sample rate. Therefore, this dataset is real measurement data, rather than a typical reanalysis dataset.

**Ningxia dataset**: The Ningxia dataset represents a mountainous area spanning from latitude 34.5°N to 42°N and longitude 106°E to 116°E. There are 30×40 grids with a grid size of 0.25 degrees in both latitude and longitude. The DEM data are collected from ETOPO1. The meteorological data are collected from ECMWF's ERA5[9], including 8 weather factors from 1/Jan/2021 to 1/Dec/2021 with 1-hour sample rate. For variable temperature, the atmosphere level is 500.

**WeatherBench dataset**: The WeatherBench dataset[10] represents a global weather dataset. We select the version with 5.625 degrees resolution, sampling rate of 6 hours, from 2008 to 2018, with five weather factors. This dataset originates from ECMWF's ERA5 as well. For variable $z$ (geopotential), the atmosphere level is 500. For variable $t$ (temperature), the atmosphere level is 850.

In the forecasting experiments, we divide each dataset into train, validation, and test sets using an 8:1:1 ratio in chronological order. The scores of the average of variables reported in Table 5 are computed based on all eight factors. Due to space limits, we only report the specific scores for four factors.

## A.2 Experimental details

We choose the learning rate at 1e-4, batch size of *PhyDL-NWP* at 10000, and hidden dimension at 100. We perform grid search in [1e-5, 1e-4, 1e-3, 1e-2, 0.1, 1, 10] for the following hyperparameters and select them as: $\alpha$ at 10, $\beta$ at 1e-2.

The neural network used for $f_\theta$ and $Q_\pi$ both consists of 8 hidden layers, where each layer has 100 neurons. MLP is the most commonly used model architecture in the literature of PINN, which leverages the universal function approximation capabilities to model complex mappings from inputs like (x, y, t) to outputs such as weather variables. This allows inference at any arbitrary resolution because the model outputs values at any real-valued coordinate, not restricted to the training grid.

We employ both automatic differentiation and finite difference (FD) methods in this paper. Specifically, once the neural network $f_\theta$ accurately approximates the weather data, we leverage PyTorch's

---

[7]ETOPO1
[8]Ningbo Meteorological Bureau
[9]ECMWF's ERA5
[10]https://mediatum.ub.tum.de/1524895

automatic differentiation to compute derivatives. PyTorch constructs a dynamic computational graph during forward operations, where each tensor records its computation history. When computing the output $y = f_\theta(t)$, invoking y.backward() enables access to the derivative with respect to $t$ via t.grad.

The finite difference (FD) method, on the other hand, is much simpler, but also much quicker. It approximates derivatives using discrete points. For the first derivative of a function $u(t)$, there are:

*A.2.1 Forward Difference.*
$$\frac{du}{dt} \approx \frac{u(t + \Delta t) - u(t)}{\Delta t} + O(\Delta t)$$

*A.2.2 Backward Difference.*
$$\frac{du}{dt} \approx \frac{u(t) - u(t - \Delta t)}{\Delta t} + O(\Delta t)$$

*A.2.3 Central Difference.*
$$\frac{du}{dt} \approx \frac{u(t + \Delta t) - u(t - \Delta t)}{2\Delta t} + O(\Delta t^2)$$

We adopt the finite difference (FD) method to compute derivatives in the weather forecasting model $g_\omega$ (Eq. 8), as automatic differentiation is not applicable—$g_\omega$ does not explicitly take time $t$ as an input, unlike $f_\theta(x, y, t)$. Another advantage is that first-order finite difference (FD) is much faster than automatic differentiation (auto-diff) because FD only requires basic arithmetic on neighboring grid points. Auto-diff has to traverse the computation graph and involves memory-heavy backward passes, especially for deep networks or large spatiotemporal inputs.

*A.2.4 Forecasting baselines.*
- PINN [30]: a physics-informed feedforward neural network that incorporates known physical laws (e.g., PDEs) as soft constraints during training to improve generalization and physical consistency.
- Bi-LSTM-T [42]: a deep learning (DL) model that uses Bi-LSTM for weather prediction.
- Hybrid-CBA [7]: a hybrid DL model that combines CNN, LSTM, and attention models for weather forecasting and correction.
- ConvLSTM [33]: a hybrid DL model that extends LSTM with convolutional gates.
- PINO [17]: a physics-informed neural operator that learns solution operators for PDEs directly, enabling efficient inference and better scalability than traditional PINNs.
- AFNO [5, 28]: a DL model that adapts Fourier neural operator for spatio-temporal modeling.

- MTGNN [40]: a DL model that learns multivariate time series with graph neural networks.
- MegaCRN [11]: a deep learning model that learns heterogeneous spatial relationships with adaptive graphs.
- ClimaX [24]: a transformer-based deep learning foundation model for weather forecasting.
- FourcastNet [28]: a foundation model for global weather forecasting based on Adaptive Fourier Neural Operators.
- GraphCast [14]: a foundation model for global weather prediction based on encoder-decoder with message passing.

Since most forecasting baselines are designed for single-step future prediction by default, we modify their neural architecture by multiplying the output dimension of the second-last layer (usually at the end of an LSTM or Conv block, before passing through the feed-forward network at the end) by the number of prediction steps. Since different baselines may operate on different resolutions of data, we will use interpolation to map to the desired resolution.

*A.2.5 Downscaling baselines.*
- Bicubic interpolation: a two-dimensional interpolation technique that uses the values and gradients of the function at surrounding grid points to obtain a smooth and continuous interpolated result.
- FSRCNN [27]: a widely recognized method in computer vision, leveraged for both downscaling and single-image super-resolution, which conducts feature mapping using multi-layer CNNs and executes upsampling via deconvolution layers.
- ResDeepD [32]: a deep model that begins with an upsampling of the input to increase dimensions before proceeding to feature mapping via ResNet.
- EDSR [10]: a deep model that first conducts feature mapping using ResNet and then performs upsampling.
- RCAN [43]: a deep model based on ResNet that incorporates a global pooling layer for channel attention.
- YNet [20]: a novel deep convolutional neural network (CNN) with skip connections and fusion capabilities to perform downscaling for climate variables.
- DeepSD [35]: a generalized stacked super resolution convolutional neural network (SRCNN) framework for statistical downscaling of climate variables.
- GINE [26]: a computer vision-based technique using topography-driven spatial and local-level information for downscaling climate simulation.